Letter

Taking the temperature of a pure quantum state

Mark T. Mitchison [1,*] Archak Purkayastha [1] Marlon Brenes [1,2] Alessandro Silva [3] and John Goold [1,†]

[1]*School of Physics, Trinity College Dublin, College Green, Dublin 2, Ireland*

[2]*Department of Physics and Centre for Quantum Information and Quantum Control, University of Toronto, 60 Saint George St., Toronto, Ontario, M5S 1A7, Canada*

[3]*SISSA, Via Bonomea 265, I-34135 Trieste, Italy*

(Received 1 July 2021; revised 3 January 2022; accepted 10 February 2022; published 8 March 2022)

Temperature is a deceptively simple concept that still raises deep questions at the forefront of quantum physics research. The observation of thermalization in completely isolated quantum systems, such as cold-atom quantum simulators, implies that a temperature can be assigned even to individual, pure quantum states. Here, we propose a scheme to measure the temperature of such pure states through quantum interference. Our proposal involves interferometry of an auxiliary qubit probe, which is prepared in a superposition state and subsequently decoheres due to weak coupling with a closed, thermalized many-body system. Using only a few basic assumptions about chaotic quantum systems, namely, the eigenstate thermalization hypothesis and the emergence of hydrodynamics at long times, we show that the qubit undergoes pure exponential decoherence at a rate that depends on the temperature of its surroundings. We verify our predictions by numerical experiments on a quantum spin chain that thermalizes after absorbing energy from a periodic drive. Our Letter provides a general method to measure the temperature of isolated, strongly interacting systems under minimal assumptions.

DOI: 10.1103/PhysRevA.105.L030201

I. INTRODUCTION

Advances in our understanding of thermodynamic concepts have always been inspired by the technologies of the time, from steam engines in the 19th century to ultracold-atom simulators in the 21st. Irrespective of the historical era, the importance of measuring temperature cannot be overstated. In 1798, the American military man and scientist, Count Rumford, noticed that he could generate heat from friction while boring cannons in the arsenal of the Bavarian army he was tasked with reorganizing. Rumford reported the systematic temperature increase of the water in which the cannon barrels were immersed [1], challenging the prevailing caloric theory of heat and inspiring Joule to perform the decisive experiments that established energy conservation as the first law of a new thermodynamic theory. In his famous paddle-bucket experiment, Joule measured the mechanical equivalent of heat by observing the temperature change induced by stirring fluid in a thermally isolated container [2]. Here, we show that recasting Joule's experiment as a fully quantum-mechanical process leads to a general scheme to measure the temperature of an isolated quantum many-body system. Our proposal relies on entangling the system with an auxiliary qubit that undergoes decoherence with a temperature-dependent rate. This thermometer scale is defined entirely through quantum interference and allows the measurement of temperature for generic systems in pure quantum states.

In the last two decades, experimental progress in cold-atom physics has enabled coherent quantum dynamics to persist over extraordinary timescales: long enough to observe isolated many-body systems thermalize without coupling to any external bath [3–7]. The emergence of thermodynamics in this context is elegantly explained by the eigenstate thermalization hypothesis (ETH) [8–10]. The ETH posits that, in a sufficiently complex and chaotic system, each energy eigenstate encodes the properties of the equilibrium ensemble. As a result, local observables in a far-from-equilibrium scenario eventually thermalize under unitary evolution [11]. The final temperature is set by the energy density of the initial condition, which may be effectively a pure quantum state. Thermal fluctuations thus arise locally because of quantum entanglement between different parts of the system [12,13] rather than by any classical statistical mixing. This begs the question: can the temperature of a pure state also be *measured* in a completely quantum-mechanical way?

Our pure-state thermometry scheme, depicted in Fig. 1, draws inspiration from Joule's pioneering experiment, for which thermal isolation was vital. We consider the extreme case of an isolated quantum system such as an ultracold atomic gas. Work is performed by changing some external constraint, thus driving the system out of equilibrium in analogy to Joule's paddles. The driving force is then removed and the system relaxes under unitary evolution. Local observables thermalize to a temperature governed by the work performed, i.e., the mechanical equivalent of heat. Joule's apparatus included an *in situ* thermometer to measure the temperature change of the insulated fluid. In our setup, this role is played by an auxiliary qubit that becomes entangled with the many-body system. Assuming only the ETH and the

*mark.mitchison@tcd.ie
†gooldj@tcd.ie

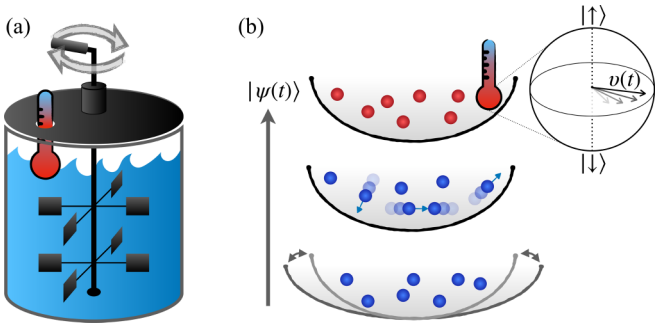

FIG. 1. Illustration of an experiment where work is performed on a thermally isolated system—such as (a) a bucket of water or (b) an ultracold atomic gas—thus driving it into a nonequilibrium state. After the external force is removed, collisions between particles lead to irreversible thermalization at a temperature determined by the energy density of the initial state, even though in panel (b) the global evolution is unitary and the system is described by a pure quantum state. The final temperature can be inferred by entangling the system to a qubit probe and measuring the resulting decoherence rate.

equations of diffusive hydrodynamics, we show that the qubit undergoes pure exponential decoherence at a temperature-dependent rate that can be interferometrically measured [14–16], providing a uniquely quantum thermometer for pure states.

Our Letter contributes to a growing body of literature seeking to establish the fundamental quantum limits of thermometry [17]. The traditional approach—used in Joule's measurements, for example—is to let the thermometer exchange energy with its surroundings and wait for equilibration. Unfortunately, this becomes challenging to implement at low temperature, where a precise thermometer needs small energy scales and correspondingly long thermalization times [18]. These drawbacks can be avoided by inferring temperature from the nonequilibrium dynamics of a probe, assuming a reliable model of the process is available [19–28]. In particular, Refs. [24–26] have shown that pure decoherence dynamics can encode temperature with a precision that is completely independent of the probe's energy. However, these proposals require the thermal system to be described by the canonical ensemble, as appropriate for an open system coupled to a heat reservoir. In contrast, our protocol offers a general solution to the problem of thermometry for isolated quantum systems, without the inherent limitations of small thermal probes that equilibrate with the system.

II. SPIN-CHAIN EXAMPLE

The quantum equivalent of Joule's paddle bucket is best illustrated by a specific example, although our scheme is general. Figure 2 details an *in silico* experiment where a thermally isolated many-body system is heated by periodic driving [29–31]. We simulate an archetypal model of a quantum chaotic system: a Heisenberg spin-$\frac{1}{2}$ chain [32,33] with Hamiltonian ($\hbar = k_B = 1$)

$$\hat{H} = J\sum_{j=1}^{L}(\hat{\sigma}_j^x\hat{\sigma}_{j+1}^x + \hat{\sigma}_j^y\hat{\sigma}_{j+1}^y + \Delta\hat{\sigma}_j^z\hat{\sigma}_{j+1}^z) + h\sum_{j\ \mathrm{odd}}\hat{\sigma}_j^z, \quad (1)$$

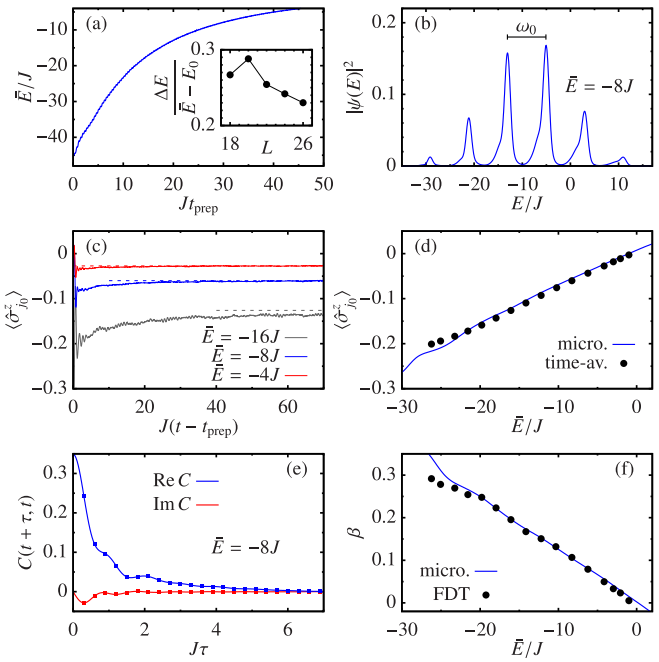

FIG. 2. Unitary heating of a quantum spin-$\frac{1}{2}$ chain. (a) Mean energy $\bar{E} = \langle\psi(t_{\mathrm{prep}})|\hat{H}|\psi(t_{\mathrm{prep}})\rangle$ of the chain as a function of the preparation time t_{prep} under local driving, $\hat{H}(t) = \hat{H} + a\sin(\omega_0 t)\hat{\sigma}_{j_0}^z$, applied to one site, j_0. Inset: Energy fluctuations, $\Delta E^2 = \langle\psi(t_{\mathrm{prep}})|(\hat{H} - \bar{E})^2|\psi(t_{\mathrm{prep}})\rangle$, vs system size at fixed temperature $T(\bar{E}) = 10J$. (b) Energy distribution of the prepared state, $|\psi(E)|^2 = \sum_n |\langle E_n|\psi(t_{\mathrm{prep}})\rangle|^2\delta(E - E_n)$, where $\hat{H}|E_n\rangle = E_n|E_n\rangle$. (c) Equilibration of the local magnetization after the drive is switched off. Solid lines show the dynamics of $\langle\hat{\sigma}_{j_0}^z\rangle$, with $\bar{E}$ increasing from the bottom to the top line. Dashed lines show the corresponding microcanonical average. (d) Time-averaged local magnetization after equilibration (black dots, obtained by time averaging over an interval $\delta t \geqslant 20J^{-1}$) compared with the microcanonical average (blue line). (e) Autocorrelation function $C(t+\tau, t)$ of the local operator $\hat{A} = \sum_j u_j\hat{\sigma}_j^z$, where $u_j \propto e^{-(j-j_0)^2}$ is a Gaussian profile ($\sum_j u_j = 1$). Lines show the real (blue/upper line) and imaginary (red/lower line) parts of $C(t+\tau, t)$ for $t - t_{\mathrm{prep}} = 100J^{-1}$, while squares indicate near-identical values for $t - t_{\mathrm{prep}} = 110J^{-1}$. (f) Inverse temperature estimated by fitting the low-frequency noise and response functions to the FDT $\tilde{\chi}''(\omega)/\tilde{S}(\omega) = \tanh(\beta\omega/2)$ (black dots) and the corresponding microcanonical prediction (blue line). Parameters: $\Delta = 0.55J$, $h = J$, $\omega_0 = 8J$, $a = 2J$.

where $\hat{\sigma}_j^{x,y,z}$ are Pauli operators pertaining to lattice site j. The exchange coupling J and anisotropy $J\Delta$, respectively, describe the kinetic and interaction energy of conserved spin excitations, while h is a staggered magnetic field that breaks integrability [34]. By exploiting Runge-Kutta methods for time evolution [35–38] and the kernel polynomial method to evaluate thermal and spectral properties [39,40], our simulations probe thermalization dynamics at system sizes beyond those accessible to exact diagonalization. Numerical methods are described in the Supplemental Material [41].

At time $t = 0$, the chain is prepared in its ground state with energy E_0. An oscillatory field is then applied locally, pumping energy steadily into the system until the drive is switched off at time t_{prep} [Fig. 2(a)]. This procedure generates a class

of nonequilibrium pure states whose average energy $\bar{E}$ can be selected by tuning the preparation time. These states have a structured energy distribution featuring sharp peaks spaced by the drive frequency [Fig. 2(b)]. Importantly, the corresponding energy fluctuations ΔE are subextensive, meaning that $\Delta E/(\bar{E} - E_0)$ decreases with system size [Fig. 2(a) inset].

After the drive is switched off, the system evolves autonomously and local observables relax to equilibrium [Fig. 2(c)], exhibiting small fluctuations around a value that is close to the prediction of the microcanonical ensemble [Fig. 2(d)]. This ensemble is characterized by a single parameter: the average energy, $\bar{E}$, with the corresponding inverse temperature $T^{-1} \equiv \beta = \beta(\bar{E})$ given by the fundamental definition $\beta(E) = d\mathcal{S}/dE$, where $\mathcal{S}(E)$ is the microcanonical entropy. Similar thermal behavior is observed in correlation functions like $C(t', t) = \langle \hat{A}(t')\hat{A}(t)\rangle - \langle \hat{A}(t')\rangle \langle \hat{A}(t)\rangle$, with $\hat{A}$ a local observable, which become approximately stationary at long times, i.e., $C(t + \tau, t) \approx C(\tau)$ [Fig. 2(e)]. Conventionally, one writes $C(\tau)$ in terms of the symmetrized noise function $S(\tau) = \mathrm{Re}\,[C(\tau)]$ and the dissipative response function $\chi''(\tau) = i\,\mathrm{Im}\,[C(\tau)]$. After relaxation, their Fourier transforms are related by the fluctuation-dissipation theorem (FDT), $\tilde{S}(\omega) = \coth(\beta\omega/2)\tilde{\chi}''(\omega)$, as expected in thermal equilibrium [Fig. 2(f)].

The thermalization of these "paddle-bucket" preparations is striking in light of the highly nonequilibrium energy distribution displayed in Fig. 2(b). Nevertheless, this behavior is completely generic and fully explained by the ETH, which can be formulated as an ansatz for the matrix elements of an arbitrary local observable, $\hat{A}$, in the energy eigenbasis [48], i.e., $A_{mn} = \langle E_m|\hat{A}|E_n\rangle$, where $\hat{H}\,|E_n\rangle = E_n\,|E_n\rangle$. The ansatz reads as

$$A_{mn} = \begin{cases} A(E_n) + O(\mathcal{D}^{-1/2}), & m = n, \\ e^{-\mathcal{S}(E_{mn})/2} f(E_{mn}, \omega_{mn}) R_{mn} + O(\mathcal{D}^{-1}), & m \neq n, \end{cases} \tag{2}$$

where $A(E_n)$ and $f(E_{mn}, \omega_{mn})$ are smooth functions of their arguments, $E_{mn} = \frac{1}{2}(E_m + E_n)$ and $\omega_{mn} = E_m - E_n$, while R_{mn} is a Hermitian matrix of random numbers with zero mean and unit variance, and $\mathcal{D}$ is the Hilbert-space dimension. See Fig. 3 for an example and Ref. [41] for further details. As is well known [11], the ETH (2) implies that any highly excited state with subextensive energy fluctuations will thermalize under unitary dynamics. More precisely, the expectation value of a local observable converges to its time average $\overline{\langle \hat{A}\rangle} = \sum_n |\langle E_n|\psi\rangle|^2 A_{nn} = A(\bar{E}) + O(\Delta E^2/\bar{E}_*^2)$, with $A(\bar{E})$ equal to the microcanonical average at inverse temperature $\beta(\bar{E})$, while the spectral function $f(\bar{E}, \omega)$ determines the noise and response functions (up to subextensive corrections) as [11,34]

$$\tilde{S}(\omega) = 2\pi \cosh(\beta\omega/2)|f(\bar{E}, \omega)|^2, \tag{3}$$

$$\tilde{\chi}''(\omega) = 2\pi \sinh(\beta\omega/2)|f(\bar{E}, \omega)|^2, \tag{4}$$

immediately implying the FDT. Although these features of the ETH have long been understood, the low-frequency behavior of the spectral function has only recently been identified as a sensitive indicator of quantum many-body chaos [49,50]. For a generic observable in a nonintegrable system, $f(E, 0)$ is nonzero and may vary significantly with temperature [Fig. 3(b)]. This observation forms the basis of our thermometry scheme.

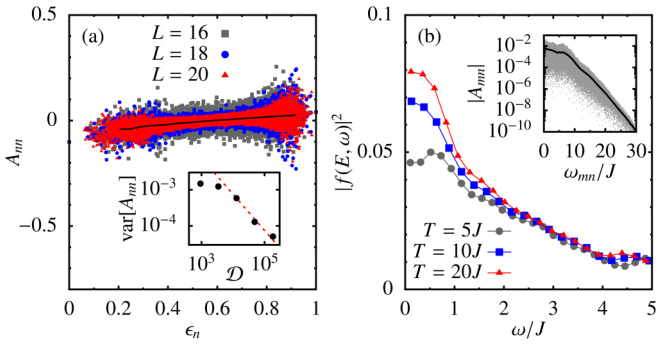

FIG. 3. Eigenstate thermalization in the staggered-field Heisenberg spin chain [see Fig. 2 caption for details]. (a) Diagonal matrix elements of the local operator $\hat{A}$ concentrate around a smooth function (black line) of the energy density, $\epsilon_n = (E_n - E_{\min})/(E_{\max} - E_{\min})$. Inset: Variance of diagonal elements evaluated within the central 10% of the spectrum for different system sizes, showing the scaling $\mathrm{var}[A_{nn}] \sim \mathcal{D}^{-1}$ (dashed red line). (b) Low-frequency spectral function for $L = 18$ and three different temperatures. Inset: Off-diagonal elements near $T = 5J$ (gray points, only 1% of elements shown) and a running average of $|A_{mn}|$ (black line).

III. THERMOMETRY PROTOCOL

Our thermometer comprises a qubit with energy eigenstates $|\uparrow\rangle$ and $|\downarrow\rangle$, coupled to the system by an interaction of the form $\hat{H}_{\mathrm{int}} = |\uparrow\rangle\langle\uparrow| \otimes g\hat{A}$ for some local observable $\hat{A}$ and coupling constant g. This kind of interaction—which can be engineered, for example, using Feshbach resonances in ultracold gases [15]—conserves the qubit's energy and ensures that it does not participate in the dynamics while in its ground state $|\downarrow\rangle$. Suppose that at time t_0, the thermal system of interest is in the pure state $|\psi(t_0)\rangle = |\psi_0\rangle$. The protocol begins by exciting the qubit into a superposition $|+\rangle = \frac{1}{\sqrt{2}}(|\uparrow\rangle + |\downarrow\rangle)$ with a $\pi/2$ pulse, preparing the joint product state $|\Psi(t_0)\rangle = |+\rangle\,|\psi_0\rangle$. In a frame rotating at the qubit precession frequency, the Schrödinger evolution is then $|\Psi(t)\rangle = \frac{1}{\sqrt{2}}(e^{-i\hat{H}(t-t_0)}\,|\downarrow\rangle\,|\psi_0\rangle + e^{-i(\hat{H}+g\hat{A})(t-t_0)}\,|\uparrow\rangle\,|\psi_0\rangle)$. Entanglement develops between the probe and the system, leading to a loss of distinguishability quantified by the fidelity between many-body system states:

$$|v(t)|^2 = |\,\langle\psi_0|e^{i\hat{H}(t-t_0)}e^{-i(\hat{H}+g\hat{A})(t-t_0)}|\psi_0\rangle\,|^2. \tag{5}$$

The resulting decrease in interference contrast is reflected in the off-diagonal elements of the qubit density matrix, $\hat{\rho}_{\mathrm{q}}(t) = \mathrm{Tr}_{\mathrm{sys}}\,|\Psi(t)\rangle\langle\Psi(t)|$, which decay in time according to $\langle\downarrow|\hat{\rho}_{\mathrm{q}}(t)|\uparrow\rangle = \frac{1}{2}v(t)$. This decoherence is finally probed by applying a second $\pi/2$ pulse with a phase θ relative to the first one, then measuring the excited-state probability of the qubit, $P_\uparrow = \frac{1}{2}\{1 + \mathrm{Re}\,[e^{i\theta}v(t)]\}$. The time-dependent overlap $v(t)$ is thus reconstructed by varying θ.

IV. PRECISION AT WEAK COUPLING

To assess the temperature dependence of the interference contrast, we focus on the weak-coupling regime and

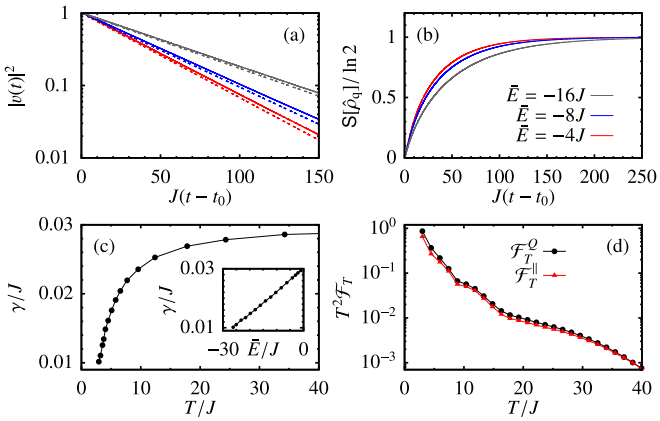

FIG. 4. Decoherence of a qubit with coupling $g = 0.2J$ to a spin-chain environment prepared in a pure thermal state as shown in Fig. 2. (a) The fidelity and (b) the entanglement entropy for three different temperatures. Solid lines show an exact calculation of Eq. (5), while the dashed lines show the weak-coupling approximation $|v(t)|^2 = e^{-\gamma(t-t_0)}$, with $\gamma = g^2\tilde{S}(0)$ extracted from dynamical calculations of $C(\tau)$. We take $t_0 - t_{\rm prep} = 100J^{-1}$ for $\bar{E} = -4J, -8J$ and $t_0 - t_{\rm prep} = 200J^{-1}$ for $\bar{E} = -16J$. In panel (a), $\bar{E}$ increases from the top to the bottom line and vice versa in panel (b). (c) Temperature dependence of the asymptotic decoherence rate, $\gamma = g^2\tilde{S}(0)$, with the energy dependence as an inset. (d) QFI (black dots) and Fisher information for a measurement in the qubit eigenbasis (red triangles), computed within the weak-coupling approximation as a function of temperature. Both quantities are evaluated at the time t^* where the QFI is maximized, i.e., $\mathcal{F}_T^Q = \mathcal{F}_T^Q(t^*) \equiv \max_t \mathcal{F}_T^Q(t)$ and $\mathcal{F}_T^{\parallel} = \mathcal{F}_T^{\parallel}(t^*)$.

approximate the fidelity (5) by a cumulant expansion to second order in g [41]. We obtain $|v(t)|^2 = e^{-\Gamma(t)}$, where

$$\Gamma(t) = 4g^2 \int \frac{d\omega}{2\pi}\, \tilde{S}(\omega) \frac{\sin^2[\omega(t-t_0)/2]}{\omega^2}. \tag{6}$$

At weak coupling, the largest effects are seen for $t - t_0 \gg \tau_c$, where τ_c is the characteristic timescale for the correlation function $C(\tau)$ to decay to zero. The integral in Eq. (6) is then dominated by the contribution near $\omega = 0$, which implies pure exponential decoherence, $|v(t)|^2 \sim e^{-\gamma(t-t_0)}$, with an asymptotic decay rate $\gamma = g^2\tilde{S}(0) \propto |f(\bar{E}, 0)|^2$. We numerically confirm this behavior in Fig. 4(a), which shows the fidelity for a probe coupled to a spin chain heated by the procedure of Fig. 2. Even for moderate coupling strengths, we observe near-perfect exponential decay with a temperature-dependent rate in close agreement with the weak-coupling prediction. The decoherence is associated with a growth in the entanglement entropy $\mathsf{S}[\hat{\rho}_q] = -\mathrm{Tr}[\hat{\rho}_q \ln \hat{\rho}_q]$, which saturates to the temperature-independent value $\mathsf{S}[\hat{\rho}_q] \to \ln 2$ characterizing a maximally entangled state [Fig. 4(b)]. This distinguishes our nonequilibrium protocol from a thermalization process. In Fig. 4(c), the temperature dependence of the decoherence rate is analyzed in more detail. We find that γ depends almost linearly on energy density [Fig. 4(c) inset], which translates into a nonlinear variation with temperature [Fig. 4(c) main panel] that is greatest at low temperatures.

We quantify the temperature information that can be extracted from our protocol using the quantum Fisher information (QFI). Consider a temperature estimate constructed from M independent measurements in a given basis, μ, on identical qubit preparations. For large M, the statistical error of any unbiased estimate is asymptotically bounded by $\Delta T^2 \geqslant 1/M\mathcal{F}_T^{\mu} \geqslant 1/M\mathcal{F}_T^Q$. Here, $\mathcal{F}_T^{\mu}$ is the Fisher information for the chosen basis while the QFI, $\mathcal{F}_T^Q = \max_{\mu} \mathcal{F}_T^{\mu}$, is the maximum over all measurements and thus describes the ultimate uncertainty limit imposed by quantum mechanics [51]. The temperature can be inferred from the exponential decay of $|v(t)|$ by measuring in the eigenbasis of $\hat{\rho}_q(t)$, i.e., by applying a final $\pi/2$ pulse with phase $\theta = -\arg v(t)$ [41]. Figure 4(d) shows the corresponding Fisher information, $\mathcal{F}_T^{\parallel}$, in the weak-coupling limit. Since $\mathcal{F}_T^{\parallel} \approx \mathcal{F}_T^Q$, we conclude that the decoherence rate captures almost all temperature information available from the probe in this example. For instance, we obtain the value $T^2\mathcal{F}_T^{\parallel} \approx 0.2$ at temperature $T = 5J$, implying that $M = 500$ measurements could suffice to achieve a precision of $\Delta T/T \gtrsim 10\%$. Note that a single ultracold gas sample may host thousands of independent impurities [15]. We emphasize that the achievable precision is independent of the qubit's energy gap, unlike a thermalized probe whose QFI depends exponentially on this gap at low temperature [18].

V. HYDRODYNAMIC DECOHERENCE

Our results show that the temperature of an isolated system can be measured using the most primitive features of quantum dynamics, namely, unitarily evolving wave functions and entanglement between subsystems. The scale of our thermometer is defined not through the energetic fluctuations of some statistical mixture, but by the rate of entanglement growth in a quantum decoherence process [52]. While this rate should generally increase with temperature, the precise dependence is system and observable specific. Nevertheless, since a generic system should display hydrodynamic behavior at long times [57], we can obtain a general form for $\gamma(T)$ assuming that the probe couples to diffusive modes of a conserved density. In $d = 3$ spatial dimensions, we obtain [41]

$$\gamma = \frac{2\bar{g}^2\chi_0 T}{D}, \tag{7}$$

where D is the diffusion coefficient, χ_0 is the thermodynamic susceptibility to long-wavelength density perturbations, and $\bar{g}$ is a renormalized coupling that depends only on the probe's spatial profile. According to Eq. (7), the qubit's decoherence rate provides an ideal, linear thermometer scale within any temperature range where D and χ_0 are approximately constant, and allows for accurate thermometry in general whenever D and χ_0 are known as a function of temperature.

In low-dimensional systems—such as our spin-chain example—similar hydrodynamic arguments predict nonexponential decoherence at intermediate times, $\Gamma(t) \sim t^{3/2}$ for $d = 1$ and $\Gamma(t) \sim t \ln t$ for $d = 2$, which crosses over to pure exponential decay, $\Gamma(t) \sim \gamma t$, when $t \gtrsim \tau_c$ [41]. The asymptotic decoherence rate γ depends on temperature as in Eq. (7), but both γ and τ_c grow with the system size for

$d < 3$ [41]. However, τ_c is too small to clearly distinguish the crossover at system sizes accessible in our simulations, where only the long-time exponential decay is observed. This interesting competition of timescales calls for further research to characterize how Markovian dynamics [48,58,59] and thermodynamics [60,61] emerge for open quantum systems in chaotic environments.

VI. CONCLUSION

Accurate, *in situ* thermometry of isolated quantum systems is an outstanding problem in cold-atom physics, where strong, short-ranged correlations confound destructive global measurement techniques such as time-of-flight imaging. Conversely, a small quantum probe facilitates local, minimally destructive temperature measurements, in principle [27,62]. Our proposal to infer temperature from decoherence dynamics does not require thermalization of the qubit or fine tuning of its energy levels, and is applicable to generic many-body systems in arbitrary states with subextensive energy fluctuations. This opens a pathway for the toolbox of quantum-enhanced thermometry [17] to probe the ultimate limit of an isolated system in a pure quantum state.

ACKNOWLEDGMENTS

We thank S. R. Clark, C. Jarzynski, A. Polkovnikov, and J. Richter for useful feedback on the Letter. M.B. and J.G. thank M. Rigol for stimulating their interest in the ETH. A.P. acknowledges funding from the European Union's Horizon 2020 research and innovation program under Marie Skłodowska-Curie Grant No. 890884. Some calculations were performed on the Lonsdale cluster maintained by the Trinity Centre for High Performance Computing. This cluster was funded through grants from Science Foundation Ireland (SFI). We acknowledge the DJEI/DES/SFI/HEA Irish Centre for High-End Computing for the provision of computational facilities, Project No. TCPHY138A. This work was supported by a SFI–Royal Society University Research Fellowship (J.G.) and the Royal Society (M.B.). J.G. and M.T.M. acknowledge funding from the European Research Council Starting Grant ODYSSEY (Grant No. 758403) and the Engineering and Physical Sciences Research Council–SFI joint project QuamNESS.

[1] B. Thompson, Philos. Trans. R. Soc. London **88**, 80 (1798).
[2] J. P. Joule, Philos. Trans. R. Soc. London **140**, 61 (1850).
[3] S. Trotzky, Y.-A. Chen, A. Flesch, I. P. McCulloch, U. Schollwöck, J. Eisert, and I. Bloch, Nat. Phys. **8**, 325 (2012).
[4] G. Clos, D. Porras, U. Warring, and T. Schaetz, Phys. Rev. Lett. **117**, 170401 (2016).
[5] A. M. Kaufman, M. E. Tai, A. Lukin, M. Rispoli, R. Schittko, P. M. Preiss, and M. Greiner, Science **353**, 794 (2016).
[6] P. Bordia, H. Lüschen, U. Schneider, M. Knap, and I. Bloch, Nat. Phys. **13**, 460 (2017).
[7] Y. Tang, W. Kao, K.-Y. Li, S. Seo, K. Mallayya, M. Rigol, S. Gopalakrishnan, and B. L. Lev, Phys. Rev. X **8**, 021030 (2018).
[8] J. M. Deutsch, Phys. Rev. A **43**, 2046 (1991).
[9] M. Srednicki, Phys. Rev. E **50**, 888 (1994).
[10] M. Rigol, V. Dunjko, and M. Olshanii, Nature (London) **452**, 854 (2008).
[11] L. D'Alessio, Y. Kafri, A. Polkovnikov, and M. Rigol, Adv. Phys. **65**, 239 (2016).
[12] S. Goldstein, J. L. Lebowitz, R. Tumulka, and N. Zanghì, Phys. Rev. Lett. **96**, 050403 (2006).
[13] S. Popescu, A. J. Short, and A. Winter, Nat. Phys. **2**, 754 (2006).
[14] M. Cetina, M. Jag, R. S. Lous, J. T. M. Walraven, R. Grimm, R. S. Christensen, and G. M. Bruun, Phys. Rev. Lett. **115**, 135302 (2015).
[15] M. Cetina, M. Jag, R. S. Lous, I. Fritsche, J. T. M. Walraven, R. Grimm, J. Levinsen, M. M. Parish, R. Schmidt, M. Knap, and E. Demler, Science **354**, 96 (2016).
[16] M. G. Skou, T. G. Skov, N. B. Jørgensen, K. K. Nielsen, A. Camacho-Guardian, T. Pohl, G. M. Bruun, and J. J. Arlt, Nat. Phys. **17**, 731 (2021).
[17] M. Mehboudi, A. Sanpera, and L. A. Correa, J. Phys. A: Math. Theor. **52**, 303001 (2019).
[18] L. A. Correa, M. Mehboudi, G. Adesso, and A. Sanpera, Phys. Rev. Lett. **114**, 220405 (2015).
[19] M. Bruderer and D. Jaksch, New J. Phys. **8**, 87 (2006).
[20] T. M. Stace, Phys. Rev. A **82**, 011611(R) (2010).
[21] C. Sabín, A. White, L. Hackermuller, and I. Fuentes, Sci. Rep. **4**, 6436 (2014).
[22] D. Hangleiter, M. T. Mitchison, T. H. Johnson, M. Bruderer, M. B. Plenio, and D. Jaksch, Phys. Rev. A **91**, 013611 (2015).
[23] S. Jevtic, D. Newman, T. Rudolph, and T. M. Stace, Phys. Rev. A **91**, 012331 (2015).
[24] T. H. Johnson, F. Cosco, M. T. Mitchison, D. Jaksch, and S. R. Clark, Phys. Rev. A **93**, 053619 (2016).
[25] S. Razavian, C. Benedetti, M. Bina, Y. Akbari-Kourbolagh, and M. G. A. Paris, Eur. Phys. J. Plus **134**, 284 (2019).
[26] M. T. Mitchison, T. Fogarty, G. Guarnieri, S. Campbell, T. Busch, and J. Goold, Phys. Rev. Lett. **125**, 080402 (2020).
[27] Q. Bouton, J. Nettersheim, D. Adam, F. Schmidt, D. Mayer, T. Lausch, E. Tiemann, and A. Widera, Phys. Rev. X **10**, 011018 (2020).
[28] D. Adam, Q. Bouton, J. Nettersheim, S. Burgardt, and A. Widera, arXiv:2105.03331.
[29] G. Bunin, L. D'Alessio, Y. Kafri, and A. Polkovnikov, Nat. Phys. **7**, 913 (2011).
[30] L. D'Alessio and M. Rigol, Phys. Rev. X **4**, 041048 (2014).
[31] A. Lazarides, A. Das, and R. Moessner, Phys. Rev. E **90**, 012110 (2014).
[32] P. N. Jepsen, J. Amato-Grill, I. Dimitrova, W. W. Ho, E. Demler, and W. Ketterle, Nature (London) **588**, 403 (2020).
[33] A. Scheie, N. E. Sherman, M. Dupont, S. E. Nagler, M. B. Stone, G. E. Granroth, J. E. Moore, and D. A. Tennant, Nat. Phys. **17**, 726 (2021).
[34] M. Brenes, S. Pappalardi, J. Goold, and A. Silva, Phys. Rev. Lett. **124**, 040605 (2020).

[35] T. A. Elsayed and B. V. Fine, Phys. Rev. Lett. **110**, 070404 (2013).
[36] R. Steinigeweg, A. Khodja, H. Niemeyer, C. Gogolin, and J. Gemmer, Phys. Rev. Lett. **112**, 130403 (2014).
[37] R. Steinigeweg, J. Gemmer, and W. Brenig, Phys. Rev. Lett. **112**, 120601 (2014).
[38] R. Steinigeweg, J. Gemmer, and W. Brenig, Phys. Rev. B **91**, 104404 (2015).
[39] A. Weiße, G. Wellein, A. Alvermann, and H. Fehske, Rev. Mod. Phys. **78**, 275 (2006).
[40] Y. Yang, S. Iblisdir, J. I. Cirac, and M. C. Bañuls, Phys. Rev. Lett. **124**, 100602 (2020).
[41] See Supplemental Material at http://link.aps.org/supplemental/10.1103/PhysRevA.105.L030201 for further details on the numerical examples, the weak-coupling expansion of the fidelity, the quantum Fisher information, and the predictions of diffusive hydrodynamics for different spatial dimensionalities, including citations to Refs. [42–47].
[42] R. Kubo, J. Phys. Soc. Jpn. **17**, 1100 (1962).
[43] L. P. Kadanoff and P. C. Martin, Ann. Phys. **24**, 419 (1963).
[44] E. Khatami, G. Pupillo, M. Srednicki, and M. Rigol, Phys. Rev. Lett. **111**, 050403 (2013).
[45] R. Mondaini and M. Rigol, Phys. Rev. E **96**, 012157 (2017).
[46] T. LeBlond and M. Rigol, Phys. Rev. E **102**, 062113 (2020).
[47] M. Brenes, T. LeBlond, J. Goold, and M. Rigol, Phys. Rev. Lett. **125**, 070605 (2020).
[48] M. Srednicki, J. Phys. A **32**, 1163 (1999).
[49] M. Brenes, J. Goold, and M. Rigol, Phys. Rev. B **102**, 075127 (2020).
[50] M. Pandey, P. W. Claeys, D. K. Campbell, A. Polkovnikov, and D. Sels, Phys. Rev. X **10**, 041017 (2020).
[51] S. L. Braunstein and C. M. Caves, Phys. Rev. Lett. **72**, 3439 (1994).
[52] Note that here we refer to entanglement between the many-body system and the probe. This is a distinct concept from the entanglement entropy between subsystems within the many-body system, which also encodes temperature in a different sense [53,54] and can be interferometrically measured [55,56].
[53] J. R. Garrison and T. Grover, Phys. Rev. X **8**, 021026 (2018).
[54] Y. O. Nakagawa, M. Watanabe, H. Fujita, and S. Sugiura, Nat. Commun. **9**, 1635 (2018).
[55] D. A. Abanin and E. Demler, Phys. Rev. Lett. **109**, 020504 (2012).
[56] H. Pichler, G. Zhu, A. Seif, P. Zoller, and M. Hafezi, Phys. Rev. X **6**, 041033 (2016).
[57] D. Forster, *Hydrodynamic Fluctuations, Broken Symmetry, and Correlation Functions* (Perseus Books, Marston Gate, 1990).
[58] C. Nation and D. Porras, Phys. Rev. E **99**, 052139 (2019).
[59] C. A. Parra-Murillo, M. Bramberger, C. Hubig, and I. De Vega, Phys. Rev. A **103**, 032204 (2021).
[60] E. Iyoda, K. Kaneko, and T. Sagawa, Phys. Rev. Lett. **119**, 100601 (2017).
[61] A. Riera-Campeny, A. Sanpera, and P. Strasberg, PRX Quantum **2**, 010340 (2021).
[62] M. Hohmann, F. Kindermann, T. Lausch, D. Mayer, F. Schmidt, and A. Widera, Phys. Rev. A **93**, 043607 (2016).